BMC Musculoskeletal Disorders

https://doi.org/10.1186/s12891-026-10186-4

Article in Press

# Effect of tendon-to-bone gap on adjustable- versus fixed-loop biceps tendon fixation

Received: 17 February 2026

Accepted: 2 July 2026

Published online: 13 July 2026

**Cite this article as:** L. G.M., S. L.M. & P. P.S. Effect of tendon-to-bone gap on adjustable- versus fixed-loop biceps tendon fixation. *BMC Musculoskelet Disord* (2026). https://doi.org/10.1186/s12891-026-10186-4

**Golovakha M. L., Lisunov M. S. & Panchenko S. P.**

# EFFECT OF TENDON-TO-BONE GAP ON ADJUSTABLE- VERSUS FIXED-LOOP BICEPS TENDON FIXATION

**Golovakha M. L., MD, PhD, DSc, Professor,** Head of the Department of Traumatology and Orthopedics, Zaporizhzhia State Medical and Pharmaceutical University, 26 Mariya Prymachenko Blvd., Zaporizhzhia, Zaporizhzhia Region, 69000, Ukraine.

**`Corresponding author email**: golovahaml@gmail.com

ORCID: 0000-0003-2835-9333

**Lisunov M. S., MD, Postgraduate student,** Department of Traumatology and Orthopedics, Zaporizhzhia State Medical and Pharmaceutical University, 26 Mariya Prymachenko Blvd., Zaporizhzhia, Zaporizhzhia Region, 69000, Ukraine

email:lisunovmykhaylo@gmail.com

ORCID: 0000-0002-4796-6019

**Panchenko S.P. Candidate of Technical Sciences, Associate Professor,** Associate Professor of the Department of Mechanical and Biomedical Engineering, Dnipro University of Technology, 19 Dmytro Yavornytskyi Avenue, Dnipro, Dnipropetrovsk Region, 49005, Ukraine

email: panchenko.s.p@nmu.one

ORCID: 0000-0001-5826-3645



**Running title:** Effect of tendon-to-bone gap on adjustable- versus fixed-loop biceps tendon fixation

**Word count:** 4923 (excluding references and figure legends);

**Figures**: 11;

**Tables**: 3.

## ABSTRACT

**Background** Distal biceps tendon ruptures significantly impair forearm flexion and supination strength, particularly in active individuals. Suspensory fixation using cortical button devices is a widely accepted surgical approach. Adjustable-loop techniques allow maximal tendon-to-bone apposition, while fixed-loop methods are simpler but may leave a gap. Biomechanical differences between these techniques specific to the distal biceps tendon remain poorly investigated, especially given the unique loading patterns of the elbow compared to other joints.

**Methods** Finite element analysis was performed using ANSYS software. Three-dimensional models of the radius and distal biceps tendon were constructed from computed tomography data. Three configurations were compared: Model 1 (adjustable-loop with dense tendon-to-bone contact, 0 mm gap), Model 2 (fixed-loop with 1.0 mm gap), and Model 3 (fixed-loop with 5.0 mm gap). Cortical bone, tendon, suture, and titanium button properties were assigned based on literature values. A 500 N tensile load was applied at the proximal tendon boundary simulating 90° elbow flexion. Stress, strain, and displacement distributions were analyzed in the fixation system and tendon.

**Results** Maximum tensile stresses in the fixation system were lowest in Model 1 (353 MPa) compared to Model 2 (407 MPa, +15%) and Model 3 (423 MPa, +20%). Tendon maximum stresses were similar across models (170–175 MPa), exceeding ultimate tendon strength only at isolated concentration nodes. Maximum strains in the fixation system followed the same pattern: 0.29 (Model 1), 0.33 (Model 2), 0.35 (Model 3). Maximum tendon displacements ($d_t$) were 5.4 mm (Model 1), 5.7 mm (Model 2), and 6.9 mm (Model 3), primarily due to suture elongation. The 90th percentile stresses ($\sigma_{P90}$) and strains ($\varepsilon_{P90}$)

remained consistent across configurations. The superior biomechanical performance of the adjustable-loop technique primarily reflects its ability to achieve zero tendon-to-bone gap rather than the loop mechanism itself.

**Conclusions** Suspensory fixation with zero tendon-to-bone gap (achieved by adjustable-loop technique) demonstrated superior biomechanical performance, exhibiting lower peak stresses, strains, and displacements in the fixation system compared to fixed-loop techniques with gaps. These findings suggest improved construct stability with zero-gap apposition. Further in vitro cyclic loading studies and clinical validation are required.

**Keywords: distal biceps tendon rupture, cortical button fixation, adjustable loop, fixed loop, finite element analysis, biomechanics, surgical treatment, elbow joint.**



## Background

Distal biceps tendon ruptures are relatively rare, with an estimated incidence of 1.2–2.5 per 100,000 population per year, predominantly affecting middle-aged men [1]. These injuries typically occur during intense physical activities, such as resistance training, but can also result from heavy lifting, falls on an outstretched arm, or anabolic steroid use [1,7], resulting in a significant reduction in forearm flexion and supination strength. This, in turn, limits daily activities and impairs quality of life. Surgical intervention remains the gold standard for restoring anatomical integrity [1] and regaining normal upper extremity function [2]. Among the various fixation methods employed in such cases, suspensory fixation using a cortical button fixator has gained widespread acceptance due to its biomechanical advantages, including high tensile strength, construct stability, and the potential for early postoperative rehabilitation.

This article presents a detailed analysis and comparison of the biomechanics of two contemporary approaches to the distal biceps tendon repair: suspensory fixation with an adjustable (variable-length) loop and with a fixed-length loop using a cortical button fixator. Both techniques have unique characteristics: the adjustable-loop method allows repair with maximal tendon apposition, which may promote superior healing and functional recovery, whereas fixed-length loops offer greater simplicity in surgical technique [3]. The choice between these approaches may influence fixation strength and stability, complication risks, and rehabilitation rates.

The relevance of this study is driven by several factors. First, despite similar clinical outcomes between the two methods, their biomechanical differences specific to the distal biceps tendon remain insufficiently investigated. Second, the elbow joint experiences unique loading patterns that differ from those in the knee joint, where analogous fixation techniques (e.g., for anterior cruciate ligament reconstruction [4,5]) have been far more extensively studied. This limits the direct extrapolation of existing data to the elbow region and underscores the need for specialised investigations, given the complex biomechanics of the elbow joint, where stability and range of motion depend on numerous factors [6]. Furthermore, the distal biceps tendon plays a critical role in everyday movements, such as forearm flexion and supination, and its rupture can lead to prolonged functional limitations if restoration is suboptimal [7].

The aim of this study is to evaluate the effect of tendon-to-bone gap magnitude on the biomechanics of cortical-button suspensory fixation of the distal biceps tendon. We hypothesized that a zero tendon-to-bone gap (achieved with the adjustable-loop technique) would result in significantly lower peak stresses, strains, and displacements within the fixation system compared with fixed-loop constructs that leave a residual gap, thereby conferring superior biomechanical stability under static tensile loading.

## Materials and Methods

The computational analysis was conducted using ANSYS software, based on the finite element method. To compare the effectiveness of different tendon fixation techniques to the radius, we constructed three-dimensional computational models that incorporated the specific features of tendon attachment in distal biceps tendon repair using the investigated methods. This resulted in two main models: Model 1 – fixation using the adjustable-loop technique (with dense tendon-to-bone contact), and Model 2 – fixation using the fixed-loop technique (with a 1.0 mm gap remaining between the tendon and the bone surface). Additionally, for comparative purposes, we created Model 3, in which fixation was performed using the fixed-loop technique but with a suture length slightly exceeding the required value, resulting in a 5.0 mm gap.

Anatomically, the region of interest was the elbow joint, formed by the humerus, ulna, and radius. The primary object of study was the biceps tendon and its behaviour under load following surgical restoration. Given that the tendon attaches distally to the radial tuberosity and proximally interacts with the shoulder girdle via the biceps muscle, the computational models were anatomically limited to the radius (Fig. 1a) and the tendon itself (Fig. 1b). Thus, we excluded the humerus and ulna, and the influence of the biceps muscle on the tendon was simulated by applying a load representative of the forces generated within it.

The positioning of the anatomical structures in the computational models corresponded to that of the upper extremity with the humerus oriented vertically downward and the forearm horizontally. Thus, elbow flexion at 90° was simulated.

Regarding the geometry of the computational models, computed tomography (CT) data were used to construct the biological components. These data were subsequently processed using specialised software and converted into digital three-dimensional models. Consequently, the shape and dimensions of the radial model accurately reflected its actual geometry, with a length of 25 cm.

The tendon model, also derived from CT images, was modeled at its average reported length of 65 mm [8]. We used CT data from an adult upper extremity.

We modeled tendon whipping and the sutures passed through the bone tunnel as a separate component (hereafter referred to as the “fixation system”; Fig. 2a), consisting of two parts. The upper part represented the whipped tendon portion as a conical hollow shell enveloping the distal tendon (Fig. 2b). The height (length) of the whipping was 40 mm, with the shell wall thickness corresponding to the suture diameter. The sutures themselves (two limbs) were modelled as two cylindrical elements, each with a diameter of 1 mm (Fig. 2c), passing through the bone tunnel. Suture lengths were varied according to the model. The whipped tendon portion was connected to the suture material model along the inferior whipping plane and the superior plane of the cylinders.

Tendon fixation was modelled by bonding the lateral surface of the distal tendon to the inner surface of the conical “whipping” model, with the distal boundaries of the tendon and whipping model coinciding. However, the distance between the distal tendon edge and the anterior bone surface varied according to the computational case. The cylindrical elements of the fixation system (suture material) passed through the bone tunnel, where they were subsequently connected to a button positioned on the posterior radial surface to secure the sutures.

The bone tunnel was created by a cylindrical cut-out at the anatomical tendon attachment site (radial tuberosity). Notably, with the described radial positioning, the tuberosity was oriented vertically upward (Fig. 3a), and thus the tunnel was formed transversely from superior to inferior (Fig. 3b). The tunnel diameter was 3.5 mm.

To replicate the investigated tendon restoration techniques in the three-dimensional numerical models, suture length varied. In Model 1, the inferior tendon edge and anterior bone surface were aligned (Fig. 4a). This configuration minimised suture length, simulating the conditions of the adjustable-loop technique, in which the surgeon uses a sliding loop to appose the tendon firmly to the bone. As the fixed-loop technique requires suture length slightly exceeding tunnel depth to allow button flipping, Model 2 incorporated a 1 mm tendon-to-bone gap (Fig. 4b), increasing suture length compared with Model 1. In Model 3, which also represented the fixed-loop technique but with excessively long sutures, the gap between the inferior tendon edge and bone was 5 mm (Fig. 4c).

The button used for suture fixation to the bone (Fig. 5) was modelled as an ellipsoidal element with two holes (for suture passage). Button length was designed to exceed the bone tunnel diameter, measuring 10 mm, with a width of 2.6 mm and thickness (height) of 1.5 mm. Hole diameters in the modelled button were 1.5 mm.

The mechanical properties assigned to the anatomical elements in the computational models corresponded to the actual properties of bone and tendon tissue as reported in the literature [9,10]. The radius comprises two types of bone tissue: the outer cortical layer (higher strength and stiffness) and the inner cancellous layer (lower stiffness). As the study focused on the tendon-bone junction behaviour, where bulk bone properties have minimal influence, cancellous tissue was not separately delineated in the three-dimensional radial model. The bone was thus assumed homogeneous and isotropic, with properties matching cortical bone throughout: modulus of elasticity (E) = $2 \times 10^4$ MPa, Poisson's ratio (ν) = 0.25 [11]. Selected biceps tendon properties were: E = 1200 MPa, ν = 0.25, ultimate strength ($\sigma_0$) = 100 MPa [10].

Suture material properties were selected based on published data: E = 1200 MPa, ν = 0.25, $\sigma_0$ = 600 MPa [12,13]. According to the manufacturer's testing data for the No. 2 FiberWire suture that is routinely used in this procedure, the ultimate failure load is 262.85 ± 20.64 N [17]. Although these values originate from manufacturer testing rather than an independent peer-reviewed study, they are consistent with independent laboratory reports of FiberWire tensile strength (approximately 263 N). The button material was modelled as titanium alloy: E = $1.15 \times 10^5$ MPa, ν = 0.35 [14,15].

The constitutive behaviour of all components was modelled using linear elastic isotropic material laws. Although the distal biceps tendon is a fibre-reinforced, anisotropic and viscoelastic tissue exhibiting a characteristic toe region, an equivalent isotropic Young's modulus of 1200 MPa (consistent with the linear portion of the stress–strain curve reported by Maganaris & Paul [10]) was assigned. This simplification is widely accepted in comparative finite element studies of tendon fixation devices, as it minimises the introduction of additional uncertain parameters while preserving the ability to rank different surgical constructs under identical loading conditions. Similarly, the suture material (E = 1200 MPa, ν = 0.25) was assigned properties corresponding to the linear region of the load–elongation curve of braided polyethylene sutures (e.g., FiberWire) within the applied load range of 500 N. The cortical bone was modelled as homogeneous and isotropic (E = $2 \times 10^4$ MPa, ν = 0.25) without separate cancellous bone layers; this approach is standard when the primary interest lies in relative stress distribution within the fixation system and tendon–bone interface, and the same bone model was used across all three configurations.

In Model 1, “dense tendon-to-bone contact” (0 mm gap) was implemented as a perfectly bonded interface between the distal tendon surface and the anterior radial cortex. Although the immediate postoperative tendon–bone interface is not yet osseointegrated, perfect bonding represents the idealised maximal apposition achieved with an adjustable-loop technique and was chosen to simulate the best-case mechanical condition intended by the surgeon. In Models 2 and 3 a physical gap was explicitly modelled between the tendon and bone.

We applied the following boundary conditions to all models. For the radial model, displacements were fully constrained (zero) at the proximal and distal epiphyses in all degrees of freedom. For the tendon model, displacements were constrained to zero on its superior surface in the horizontal plane, while vertical displacements were permitted. It should be noted that, mechanically, both tendon and suture material resist tension only (offering no compression resistance); the applied constraints ensured these operational conditions.



Loading and boundary conditions were chosen to represent the primary physiological loading direction of the distal biceps tendon at 90° elbow flexion. A resultant tensile force of 500 N was applied as a uniformly distributed pressure across the entire superior cross-sectional surface of the tendon model, thereby simulating muscle pull transmitted through the musculotendinous junction and avoiding artificial stress singularities associated with a point load. According to the biomechanical study by Shukla et al. [16], failure loads at 90° flexion average 643 N (SE 161 N); therefore, the selected 500 N load is submaximal. This 500 N load is below the estimated failure load of the entire two-suture construct (approximately 525 N) commonly used in the procedure. Both proximal and distal epiphyses of the 25-cm radius model were fully constrained in all degrees of freedom to prevent rigid-body motion and ensure numerical stability – a standard approach in comparative finite-element analyses of isolated forearm segments. Although the distal biceps tendon also acts as a forearm supinator, the present study intentionally modelled pure axial loading; because a linear-elastic material model was used and identical boundary conditions were applied to all three configurations, the relative ranking of the fixation techniques remains valid across a range of loads.

For orientation within the computational models and description of results, an XYZ coordinate system was employed (Fig. 7), with X and Y axes in the horizontal plane and the Z axis directed vertically from inferior to superior, perpendicular to the XOY plane.

Mesh generation was performed using the capabilities of the employed software package. A maximum element size of 1 mm was specified for all model components (Fig. 8).

To ensure the reliability of the numerical results, a preliminary mesh convergence study was performed. The adopted maximum element size of 1 mm was chosen after testing coarser (2 mm) and finer (0.5 mm) meshes. The difference in peak stresses ($\sigma_{max}$) and strains ($\varepsilon_{max}$) between the 1 mm and 0.5 mm meshes was less than 4% in the fixation system and less than 6% in the tendon, confirming that the chosen mesh density provides sufficient accuracy for comparative analysis. All three models (1–3) were generated using identical mesh parameters, guaranteeing the validity of direct comparison between the adjustable- and fixed-loop configurations. Although the distal biceps tendon is known to exhibit anisotropic and viscoelastic behaviour, an isotropic linear-elastic material model (E = 1200 MPa) was employed, consistent with previously published FEA studies of tendon fixation. This simplification is acceptable for relative biomechanical comparison and does not affect the ranking of the fixation techniques.

## Results

The performed numerical experiment yielded distribution patterns of stress-strain state components within the elements of the computational models. To evaluate the effectiveness of the investigated biceps tendon fixation methods in terms of junction strength and stiffness, the magnitudes of stresses, strains, and displacements in the fixation system and the tendon were selected as criteria. The obtained results are presented in Tables 1, 2, and 3.

Regarding the stress indicators arising in the investigated components of the numerical repair models, the following observations were made. The stress state was markedly heterogeneous, with stresses varying in both magnitude and direction at each point in the model.

Given the loading scheme employed in the constructed models and the mechanical behaviour of the tendon and sutures, a preliminary analysis of stress distribution was conducted. This revealed that the predominant stresses in the investigated elements were normal tensile stresses ($\sigma_z$) acting in the direction of the applied force (vertical direction). Accordingly, Table 1 summarises the normal stress values arising in the fixation system and tendon along the z-axis of the selected coordinate system, depending on the computational case.

It should be noted that Table 1 presents three stress values for each investigated element. This tabular format highlights the heterogeneity of the stress state and facilitates a more detailed description of the results. The following designations are used: $\sigma_{max}$ – the highest stress magnitude obtained in the individual component; $\sigma_{P90}$ – the 90th percentile stress value across the investigated element, $\sigma_{Mis}$ – equivalent stress (von Mises).

**Table 1.** Stresses in the components of the computational models (MPa). σ_max – maximum stresses; σ_P90 – the 90th percentile stress; σ_Mis – equivalent von Mises stress.

| Model | Fixation system (suture material) | | | Tendon | | |
|---|---|---|---|---|---|---|
| | σ_max | σ_P90 | σ_Mis | σ_max | σ_P90 | σ_Mis |
| 1 (dense tendon-to-bone contact) | 353 | 10 | 349 | 175 | 10 | 214 |
| 2 (fixed-loop length, 1.0 mm gap) | 407 | 10 | 395 | 175 | 10 | 208 |
| 3 (fixed-loop length, 5.0 mm gap) | 423 | 10 | 420 | 170 | 10 | 205 |

As evident from Table 1, the longitudinal stresses (σ_z) in the fixation systems across the different computational models were 2–2.5 times greater than the corresponding values in the tendon. The highest stresses in the fixation system for Model 1 (dense tendon-to-bone contact) were the lowest among the σ_max values for this component in the other models. In Model 2 (fixed-loop length, 1.0 mm gap), these stresses increased by 15%, and in Model 3 (fixed-loop length, 5.0 mm gap), they rose by a further 4%, being 20% higher than in Model 1. However, in the tendon, maximum stress magnitudes remained nearly consistent across all computational cases: identical in Models 1 and 2, and 3% lower in Model 3.



Regarding the 90th percentile stress indicators (σ_P90), their magnitudes were consistent across both investigated components irrespective of the computational case (Models 1, 2, and 3). It should be clarified that, in this study, 90th percentile stresses refer to the highest stresses occurring in the individual model element but not coinciding with the maximum stress values (σ_max).

Further clarification is required: maximum stresses ($\sigma_{max}$) in each component were obtained at specific points (nodes of the finite element mesh), namely in stress concentration zones. Away from these points, longitudinal stress ($\sigma_z$) magnitudes decreased substantially, with a more uniform distribution. Thus, in Table 1, the 90th percentile stress indicators ($\sigma_{P90}$) represent the value not exceeded by stresses at all other points (except $\sigma_{max}$) in the investigated element of the computational configuration.

Table 1 shows that, in the fixation system, maximum stresses were 35–42 times greater than the 90th percentile stresses, depending on the computational case. For the tendon, this difference was approximately 17-fold across all constructed models.

Examining the stress distribution patterns in the model components, maximum stresses ($\sigma_{max}$) in the fixation systems occurred in the portion simulating the suture material (Fig. 9a). In the portion representing tendon whipping, longitudinal stresses ($\sigma_z$) were substantially lower and, as noted, did not exceed the 90th percentile stress values ($\sigma_{P90}$).



Regarding the stress state in the tendon, the distribution of normal stresses ($\sigma_z$) was more uniform than in the fixation system, with minor concentration zones (Fig. 9b). Maximum stresses arose in the inferior portion of the tendon model, with normal stress ($\sigma_z$) magnitudes decreasing with increasing z-coordinate (in the proximal direction).

Analysis of absolute stress magnitudes revealed that maximum stresses ($\sigma_{max}$) in the investigated components of the computational models reached substantial levels. Specifically, in the tendon, maximum stresses exceeded its ultimate strength ($\sigma_0$) by 75% in Models 1 and 2, and by 70% in Model 3. However, in the fixation system elements (suture material), the highest stresses were below the ultimate strength ($\sigma_0$), providing a safety margin of 1.7-fold (Model 1), 1.5-fold (Model 2), and 1.4-fold (Model 3), depending on the computational case. It should be reiterated that maximum stress ($\sigma_{max}$) values were obtained at isolated nodes in the investigated model components; even at minimal distances (a few finite elements) from these nodes, maximum stress magnitudes decreased substantially and did not exceed the ultimate strength of each component. Furthermore, at more distant points (nodes) relative to concentration zones, stress values did not exceed the 90th percentile stress magnitudes ($\sigma_{P90}$), which were significantly below the ultimate strength ($\sigma_0$) of the respective material. Thus, it can be concluded that strength conditions are satisfied overall for each constituent of the computational configuration and for the entire biceps tendon repair system.

Table 2 presents the relative strain values in the investigated components of the numerical models. It should be noted that Table 2 follows the same structure as Table 1, but providing two values for each element depending on the computational case: $\varepsilon_{max}$ – maximum strain; $\varepsilon_{P90}$ – 90th percentile strain.

Furthermore, based on the stress state analysis results, Table 2 shows the magnitudes of relative longitudinal strains ($\varepsilon_z$) arising in the direction of the applied load.

**Table 2.** Strains in the components of the computational models. $\varepsilon_{max}$ – maximum strains; $\varepsilon_{P90}$ – 90th percentile strain.

| Model | Fixation system | | Tendon | |
|---|---|---|---|---|
| | $\varepsilon_{max}$ | $\varepsilon_{P90}$ | $\varepsilon_{max}$ | $\varepsilon_{P90}$ |
| 1 (dense tendon-to-bone contact) | 0.29 | 0.01 | 0.12 | 0.01 |

| Model | Fixation system | | Tendon | |
|---|---|---|---|---|
| 2 (fixed-loop length, 1.0 mm gap) | 0.33 | 0.01 | 0.12 | 0.01 |
| 3 (fixed-loop length, 5.0 mm gap) | 0.35 | 0.01 | 0.12 | 0.01 |

As evident from Table 2, similar to the maximum stress indicators (σ_max), the maximum strain magnitudes (ε_max) in the fixation system were greater than those in the tendon model. The difference in maximum strain (ε_max) between the investigated components was 2.4-fold (Model 1), 2.8-fold (Model 2), and 2.9-fold (Model 3), depending on the computational case.

The lowest maximum strain value (ε_max) in the fixation system was obtained in Model 1 (adjustable-loop length, dense tendon-to-bone contact). In computational case 2 (fixed-loop length, 1.0 mm gap), the maximum strain magnitude was 14% higher, and in Model 3 (fixed-loop length, 5.0 mm gap), it was 21% higher. As with maximum stress (σ_max), maximum relative strains (ε_max) in the tendon were consistent across all computational configurations. Additionally, 90th percentile strain magnitudes (ε_P90), like 90th percentile stresses (σ_P90), did not differ across all numerical models for both investigated components. However, in contrast to the difference between maximum (σ_max) and 90th percentile (σ_P90) stresses, the disparity between maximum (ε_max) and 90th percentile (ε_P90) strains was somewhat smaller: 29-, 33-, and 35-fold in the fixation system depending on the computational case, and 12-fold in the tendon across all constructed models.

Regarding the pattern of the deformed state in the investigated components, it fully corresponded to the stress distribution pattern. The highest longitudinal strains (ε_z) in the fixation system occurred in the sutures and gradually decreased in the portion modelling tendon whipping (Fig. 10a). Maximum strain magnitudes in the tendon were located in the distal portion and decreased proximally (Fig. 10b).

As an additional parameter for assessing tendon fixation stiffness, the displacements (d) of model points in the direction of the applied load (physiological direction) were selected (Table 3).

It should be noted that, unlike Tables 1 and 2, Table 3 presents only maximum displacement values (max), without 90th percentile indicators (P90). This tabular format was chosen because evaluating tendon fixation stability requires comparing the highest point displacements, which identify the stiffer system. Additionally, further analysis of displacement distribution in the investigated elements indicated that displacements primarily resulted from suture deformation (inferior portion of the fixation system model). Deformation in the proximal fixation system portion (whipping section) and the tendon was minimal.

**Table 3.** Displacements in the components of the computational models (mm)

| **Model** | **Fixation system d_f** | **Tendon d_t** |
|---|---|---|
| 1 (dense tendon-to-bone contact) | 5.2 | 5.4 |
| 2 (fixed-loop length, 1.0 mm gap) | 5.5 | 5.7 |
| 3 (fixed-loop length, 5.0 mm gap) | 6.7 | 6.9 |

Regarding displacements in the fixation system (d_f), the greatest shifts in its distal portion (suture material) occurred at the junction of each suture with the whipping zone. The superior portion of the fixator model (whipping section) displaced almost as a rigid body, with negligible differences between superior and inferior fragment displacements (Fig. 11a).

For tendon displacements (d_t), as this component is stiffer than the fixation system – particularly the suture-modelled portion – tendon point displacements, like those in the superior fixation system portion, primarily resulted from suture deformation, behaving as a rigid body. Thus, points in the superior and inferior tendon portions displaced by nearly identical magnitudes, without substantial tendon deformation (Fig. 11b).

Based on this, it was decided not to separately investigate displacement indicators at all other model points (beyond maximum values) or include them in Table 3.

It should be reiterated that, in reality, displacement magnitudes at different model points varied from the maximum depending on their vertical position, though not substantially. The exception was the fixation system portion modelling the suture material, where displacements ranged from 0 at the suture-button junction to the maximum at the transition to whipping.

Analysis of displacement magnitudes showed that maximum values in the fixation system and tendon coincided in each computational model case. As seen in Table 3, transitioning from adjustable-loop to fixed-loop tendon repair increased absolute displacement magnitudes. The lowest maximum displacements were obtained in the adjustable-loop repair model with dense tendon-to-bone contact, equalling 5 mm. In Model 2 (fixed-loop length, 1.0 mm tendon-to-bone gap), this increased by 20%, and in Model 3 (fixed-loop length, 5.0 mm gap), by 40%, compared with Model 1.

## Discussion

The biomechanics of the elbow joint represent a complex system involving the interaction of various biological structures – bones and soft tissues (ligaments, muscles, and tendons) – each playing a crucial role in full upper extremity function. In particular, the distal tendon of the biceps brachii ensures stability and strength during forearm flexion and supination movements; thus, its injury leads to substantial limb dysfunction and necessitates a careful approach to treatment selection [18]. Suspensory fixation with a cortical button allows achievement of high construct strength and facilitates early recovery of the injured limb's function, which is critical for preventing muscle atrophy and joint contracture development. This method is gaining increasing popularity and undergoing numerous modifications [19,20]. Specifically, the choice between fixed- and adjustable-loop lengths may influence parameters such as resistance to cyclic loading, the risk of gap formation between tendon and bone, and the maximum load the fixation construct can withstand before failure [18].

When creating the bone tunnel at the radial tuberosity during actual surgery, care must be taken to protect the posterior interosseous nerve, which lies in close proximity to the drill path. Although the present finite element study focused on mechanical performance and did not model neurovascular structures, this anatomical consideration is clinically important and should be addressed during intraoperative tunnel placement to minimise the risk of iatrogenic nerve injury.



It is important to note that the present study simultaneously evaluated the effect of loop type and the magnitude of the tendon-to-bone gap. The adjustable-loop technique (Model 1) was modelled with complete (0 mm) apposition, which is its primary clinical advantage. In contrast, the fixed-loop models (Models 2 and 3) incorporated 1.0 mm and 5.0 mm gaps, respectively, reflecting the typical surgical outcome of fixed-length constructs. Thus, the superior biomechanical performance of Model 1 cannot be attributed solely to the adjustable-loop mechanism per se, but rather to the combination of loop adjustability and the resulting zero-gap apposition. The study is therefore best interpreted as an investigation of the biomechanical influence of tendon-to-bone gap size in suspensory fixation, with the adjustable-loop technique representing the most reliable clinical method to achieve optimal contact.

The results of the numerical modelling indicate that the fixation technique employing an **adjustable-loop length** with dense tendon-to-bone contact (Model 1) provided superior biomechanical performance compared with the fixed-loop technique associated with gaps of 1.0 mm and 5.0 mm (Models 2 and 3, respectively). A comparison of the von Mises equivalent stress values and other components of the stress state reveals that the highest values are attained by normal stresses acting in the direction of the z-axis (vertical direction). Specifically, maximum normal stresses $\sigma_z$ in the fixation system (suture material) were 353 MPa in Model 1, which was 13% lower than in Model 2 (407 MPa) and 17% lower than in Model 3 (423 MPa), whereas tendon stresses remained comparable (175 MPa in Models 1 and 2; 170 MPa in Model 3). These findings suggest reduced stress concentration in the fixation system under dense apposition, potentially lowering the risk of construct failure under a 500 N load.

Tendon stresses exceeded the ultimate strength, but these peaks occurred solely at stress concentration nodes, with rapid decline away from them. In the fixation system, maximum stresses remained below the suture material's ultimate strength, providing a safety margin. These peaks are artefactual mesh concentrations and do not represent realistic failure.

Although maximum tensile stresses in the tendon reached 170–175 MPa and thereby exceeded the literature-reported ultimate tensile strength (100 MPa), these peak values occurred exclusively at isolated nodal points of stress concentration at the distal tendon edge and the tendon–suture whipping junction. As previously noted in the mesh convergence analysis (see

Materials and Methods), such local singularities are well-recognised artefacts of the finite-element method at geometric discontinuities and do not reflect the stress state in the bulk of the tendon. Stresses away from these concentration nodes remained well below the ultimate strength. In the fixation system the safety margin for the suture material was 1.4–1.7-fold under the applied static load. It should be emphasised that the present model considered only a single static load of 500 N; cyclic loading, which governs clinical fatigue failure of sutures, was not simulated. Therefore, the reported safety margins cannot be directly extrapolated to long-term in vivo durability.

The observed lower peak stresses, strains and displacements in the adjustable-loop configuration (Model 1) indicate superior mechanical stability and reduced risk of gap formation under static conditions compared with fixed-loop techniques. However, any potential clinical benefits regarding healing or rehabilitation remain speculative, as biological processes of tendon-to-bone integration were not addressed in this purely biomechanical study. These advantages should be confirmed in future in vitro cyclic-loading experiments and clinical trials.

Additionally, 90th percentile stresses ($\sigma\_P90 \approx 10$ MPa) were stable across all models in both components, confirming overall construct integrity, though localised concentrations highlight the need to consider focal effects in clinical practice.

Consistent with stress patterns, relative strains ($\varepsilon$) in the fixation system were lowest in Model 1 ($\varepsilon\_max = 0.29$), increasing by 14% in Model 2 (0.33) and 21% in Model 3 (0.35), while tendon strains remained unchanged at 0.12 across all cases. This indicates greater stability with dense contact fixation compared with fixed-length sutures. Strain distribution, with maxima in the inferior suture portion decreasing proximally, aligns with the tensile mechanics of tendons.

The most pronounced difference was in maximum displacements: 5 mm in Model 1 versus 6 mm (20% increase) in Model 2 and 7 mm (40% increase) in Model 3, primarily due to suture deformation rather than tendon or whipping section deformation. This enhanced stiffness in Model 1 may reduce the risk of tendon-bone diastasis.

The obtained numerical results are consistent with the literature, where cortical button fixation demonstrates superior strength compared with suture anchors or interference screws for distal biceps tendon repair [18]. However, direct comparisons of adjustable versus fixed loops specific to the elbow are scarce. In contrast to anterior cruciate ligament (ACL) biomechanical studies, where adjustable loops [21] exhibit greater elongation under cyclic loading, the unique loading patterns of the elbow (flexion and supination) preclude direct extrapolation from knee data. This underscores the novelty of the present study. Nonetheless, the models have limitations: simplified geometry (radius and tendon only, excluding humerus/ulna), static rather than cyclic loading, and isotropic material properties ($E = 2 \times 10^4$ MPa for bone; 1200 MPa for tendon), potentially underestimating real-world conditions in distal biceps restoration, necessitating more advanced models and experiments. Notably, calculations for supination movements and cyclic loading were not performed. Despite these simplifications, the advantages of the adjustable-loop fixation were evident even under static conditions. Furthermore, further in vitro or clinical studies are required to validate these numerical findings.

A potential limitation of the present study is that the anatomical geometry of the radius and distal biceps tendon was derived from a single CT scan of a middle-aged male. Consequently, any individual anatomical idiosyncrasies are propagated equally across all three models. However, because the same geometry was used for Models 1–3, inter-specimen variability was eliminated, allowing the isolated evaluation of the effect of tendon-to-bone gap size on fixation biomechanics. Although a geometric sensitivity analysis with multiple CT datasets or a population-averaged model would further enhance the generalisability of the findings, such an analysis was beyond the scope of this initial comparative investigation.

Analysis of unresolved scientific questions reveals a paucity of clinical and experimental – particularly numerical – studies directly comparing these two fixation methods for the distal biceps tendon in terms of strength, stability, and healing influence. Other potential risks remain unexplored, including adjustable-loop elongation under cyclic loading and the impact of precise tension adjustment on tendon regeneration and restoration of normal elbow biomechanics. Investigating these aspects could significantly refine surgical techniques and optimise patient outcomes, particularly in active individuals prioritising rapid and complete upper extremity functional recovery. The lack of comprehensive data on the biomechanical characteristics of fixed and adjustable loops in the context of the distal biceps tendon emphasises the need for continued research.



In a clinical context, the novel technique may optimise treatment for active patients by reducing rehabilitation time and complication risks, facilitating full upper extremity functional restoration. Thus, this work not only examines the biomechanical advantages and disadvantages of the two repair methods but also highlights gaps in current knowledge requiring further investigation. These analytical results may serve as a foundation for developing recommendations on the optimal surgical approach for distal biceps tendon ruptures. This article contributes to addressing these issues by providing a detailed overview of contemporary fixation methods and analysing their potential for treatment optimisation.

Although the current study evaluated only initial (static) fixation stability, we expect that the superior biomechanical performance of zero-gap adjustable-loop fixation may translate into better tendon-to-bone healing, lower rates of gap formation, and improved long-term functional outcomes. These hypotheses, however, require confirmation in mid- and long-term clinical studies with radiographic and functional assessment.

## Conclusions

Finite element biomechanical modelling has demonstrated that suspensory fixation with zero tendon-to-bone gap (achieved by the adjustable-loop technique) resulted in the lowest peak stresses, strains and displacements in the fixation system. This advantage primarily reflects its ability to achieve zero tendon-to-bone gap rather than the loop mechanism itself. Ultimate validation requires further in vitro cyclic loading studies and clinical trials.

## Declarations

### Abbreviations

ACL: anterior cruciate ligament

CT: computed tomography

FEA: finite element analysis

PIN: posterior interosseous nerve

### Ethics approval and consent to participate

The materials of the study were reviewed at a meeting of the Bioethics Commission of Zaporizhzhia State Medical and Pharmaceutical University (protocol dated 11 June 2026, No. 9). The Commission concluded that the study does not violate bioethical norms. All experiments and procedures described in this study were performed in accordance with the Declaration of Helsinki and relevant guidelines and regulations.

**Consent for publication**

Not applicable.

**Availability of data and materials**

The datasets generated and/or analysed during the current study are available from the corresponding author on reasonable request.

**Competing interests**

The authors declare that they have no competing interests.

**Funding**

No funding was received for this study.

**Authors' contributions**

Golovakha M.L. was the project leader, developed the overall concept of the study, served as a consultant for the researchers, defined the study design, reviewed and edited the manuscript after writing, and finalized its final version.

Lisunov M.S. justified the relevance of the study, conducted the analysis of existing literature, determined the initial data for model construction, served as a consultant during model building, performed the analysis and interpretation of the obtained data, and wrote all sections of the manuscript.

Panchenko S.P. performed the construction of the finite element models and directly obtained the biomechanical parameters.

All authors read and approved the final manuscript.

**Acknowledgements**

Not applicable.

**References**

1. Jaschke M, Rekawek K, Sokolowski S, Kolodziej L. Distal biceps tendon rupture: a comprehensive overview. EFORT Open Rev. 2023;8(7):509-20. doi:10.1530/EOR-23-0035.

2. Boufadel P, Daher M, Lopez R, Fares MY, Lawand J, Khan AZ, Abboud JA. Return to sport after distal biceps tendon repair: a systematic review. Am J Sports Med. 2025;53(7):1769-78. doi:10.1177/03635465241295618.

3. Campbell ST, Liu J, Gowd AK, Amin N, Sardelli M, Morrison M. Does retensioning of adjustable-loop cortical suspension devices improve performance: a systematic review and meta-analysis. J Arthrosc Surg Sports Med. 2024;5(1):3-11. doi:10.25259/JASSM_22_2022.

4. Elmholt SB, Nielsen TG, Lind M. Fixed-loop vs. adjustable-loop cortical button devices for femoral fixation in ACL reconstruction – a systematic review and meta-analysis. J Exp Orthop. 2022;9:106. doi:10.1186/s40634-022-00544-1.

5. Alarifi SM, Herrington LC, Althomali OW, Alenezi F, Bin Sheeha B, Jones RK. Biomechanical analysis after anterior cruciate ligament reconstruction at the return-to-sport time point. Orthop J Sports Med. 2025;13(5):23259671251340302. doi:10.1177/23259671251340302.

6. Strafun S, Levadnyi I, Makarov V, Awrejcewicz J. Comparative biomechanical analysis of stress-strain state of the elbow joint after displaced radial head fractures. J Med Biol Eng. 2018;38(4):618-24. doi:10.1007/s40846-017-0334-1.

7. Wörner EA, Nagel M, Kodde IF, Eygendaal D, The B. Return to sports following distal biceps tendon repair: a current concepts review. J ISAKOS. 2023;8(4):227-31. doi:10.1016/j.jisako.2023.02.004.

8. Kulshreshtha R, Singh R, Sinha J, Hall S. Anatomy of the distal biceps brachii tendon and its clinical relevance. Clin Orthop Relat Res. 2007;456:117-20. doi:10.1097/BLO.0b013e31802f78aa.

9. Junno JA, Niinimäki S, Niskanen M, Nunez M, Tuukkanen J. Cross sectional properties of the human radial tuberosity. Homo. 2011;62(6):459-65. doi:10.1016/j.jchb.2011.08.009.

10. Maganaris CN, Paul JP. In vivo human tendon mechanical properties. J Physiol. 1999;521(Pt 1):307-13. doi:10.1111/j.1469-7793.1999.00307.x.

11. Beisekenov N, Sadenova M, Azamatov B, Syrnev B. Analysis of biomechanical characteristics of bone tissues using a Bayesian neural network: a narrative review. J Funct Biomater. 2025;16(5):168. doi:10.3390/jfb16050168.

12. Scherman P, Haddad R, Scougall P, Walsh WR. Cross-sectional area and strength differences of Fiberwire, Prolene, and Ticron sutures. J Hand Surg Am. 2010;35(5):780-4. doi:10.1016/j.jhsa.2010.02.005.

13. Alden A. Finite element modeling and experimental characterization of knot configuration effect on the mechanical performance of surgical suture [dissertation]. Kalamazoo (MI): Western Michigan University; 2018. Available from: https://scholarworks.wmich.edu/dissertations/3375.

14. Golovakha ML, Orljanski W, Benedetto KP, Panchenko S, Büchler P, Henle P, Aghayev E. Comparison of theoretical fixation stability of three devices

employed in medial opening wedge high tibial osteotomy: a finite element analysis. BMC Musculoskelet Disord. 2014;15:230. doi:10.1186/1471-2474-15-230.

15. Lee YT, Peters M, Welsch G. Elastic moduli and tensile and physical properties of heat-treated and quenched powder metallurgical Ti-6Al-4V alloy. Metall Trans A. 1991;22(3):709-14. doi:10.1007/BF02670293.

16. Shukla DR, Morrey BF, Thoreson AR, An KN, O'Driscoll SW. Distal biceps tendon rupture: an in vitro study. Clin Biomech (Bristol, Avon). 2012;27(3):263-7. doi:10.1016/j.clinbiomech.2011.09.010.

17. Arthrex, Inc. FiberWire® vs Dynacord™ orthopedic sutures: a performance comparison. 2024. (Manufacturer data) Available from: https://www.arthrex.com/es/recursos/LA1-000181-en-US/fiberwire-vs-dynacord-orthopedic-sutures-a-performance-comparison?referringteam=shoulder. Accessed 27 Oct 2025.

18. Taylor AL, Bansal A, Shi BY, Best MJ, Huish EG, Srikumaran U. Optimizing fixation for distal biceps tendon repairs: a systematic review and meta-regression of cadaveric biomechanical testing. Am J Sports Med. 2021;49(11):3125-31. doi:10.1177/0363546520986999.

19. Ernstbrunner L, Almond M, Rupasinghe HS, Jo OI, Zbeda RM, Ackland DC, Ek ET. Biomechanical comparison of distal biceps tendon repair techniques: extracortical single-button inlay fixation versus intracortical double-button onlay anatomic footprint fixation. Am J Sports Med. 2023;51(7):1895-903. doi:10.1177/03635465231171131.

20. Majumdar A, Salas C, Chavez W, Bankhead C, Sapradit TJ, Mercer D, Wascher DC, Richter DL. No significant difference between intramedullary and extramedullary button fixation for distal biceps brachii tendon rupture after cyclic loading in a cadaver model. Arthrosc Sports Med Rehabil. 2021;3(3):e807-13. doi:10.1016/j.asmr.2021.01.022.

21. Smith PA, Piepenbrink M, Smith SK, Bachmaier S, Bedi A, Wijdicks CA. Adjustable- versus fixed-loop devices for femoral fixation in ACL reconstruction: an in vitro full-construct biomechanical study of surgical technique-based tibial fixation and graft preparation. Orthop J Sports Med. 2018;6(4):2325967118768743. doi:10.1177/2325967118768743

**Figure legends**

Fig. 1 Anatomical components of the computational models.

(a) Three-dimensional model of the radius (length 25 cm) constructed from computed tomography (CT) data. (b) Model of the distal biceps brachii tendon with an average reported length of 65 mm.

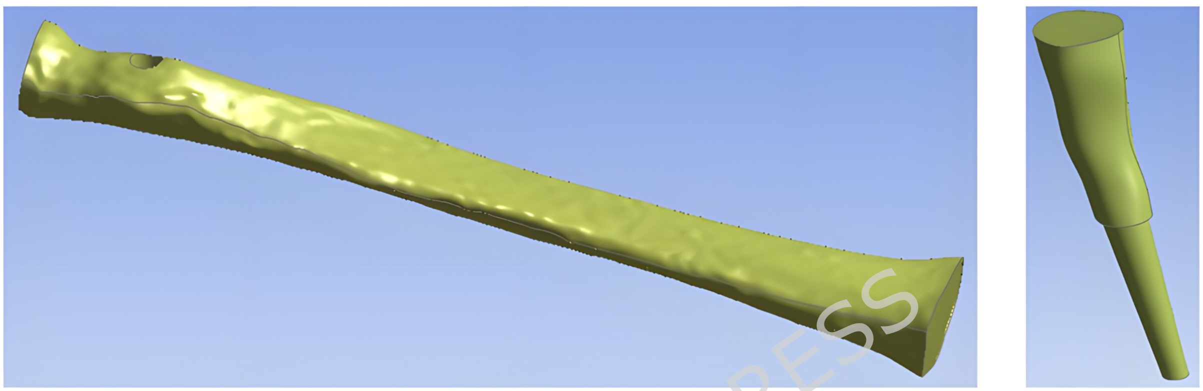

a) b)

ARTICLE IN PRESS

Fig. 2 Biceps tendon fixation system model.

(a) Overall view of the fixation construct. (b) Conical hollow shell representing the whipped tendon portion (whipping length 40 mm, wall thickness corresponding to suture diameter). (c) Two cylindrical elements modelling the suture limbs (diameter 1 mm each).

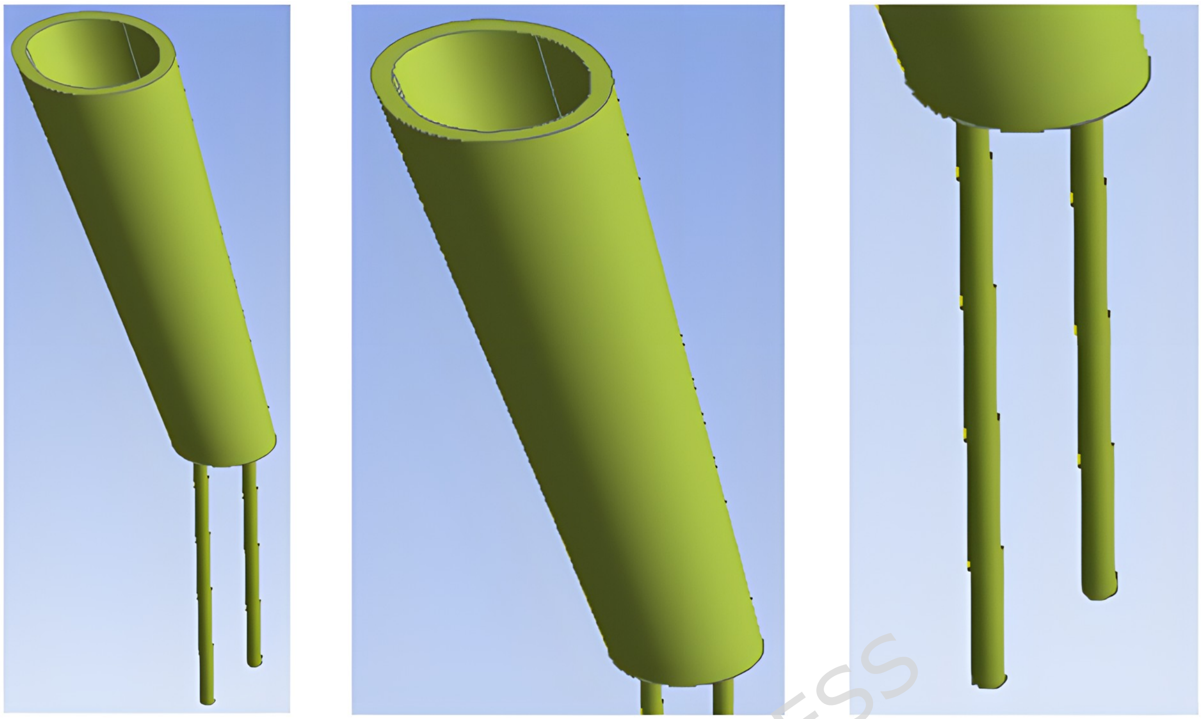

a) b) c)

Fig. 3 Views of the radius model.

(a) Lateral view showing the radial tuberosity oriented vertically upward. (b) Superior view illustrating the transverse bone tunnel (diameter 3.5 mm) at the anatomical tendon attachment site.

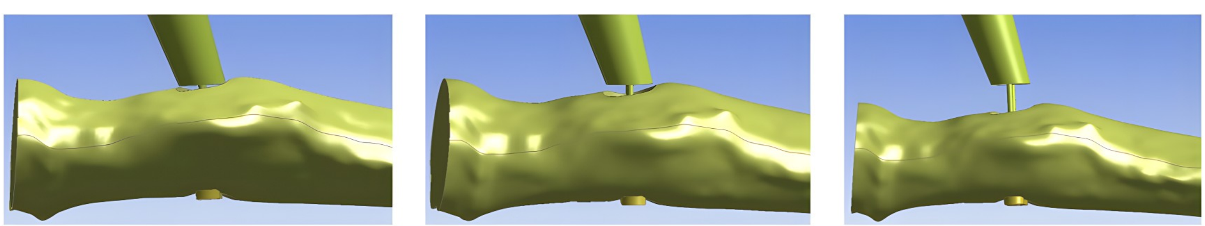

a) b) c)

Fig. 4 Differences in tendon-to-bone apposition across computational configurations.

(a) Model 1: adjustable-loop technique with dense tendon-to-bone contact (0 mm gap). (b) Model 2: fixed-loop technique with 1.0 mm tendon-to-bone gap. (c) Model 3: fixed-loop technique with excessively long sutures resulting in 5.0 mm tendon-to-bone gap.

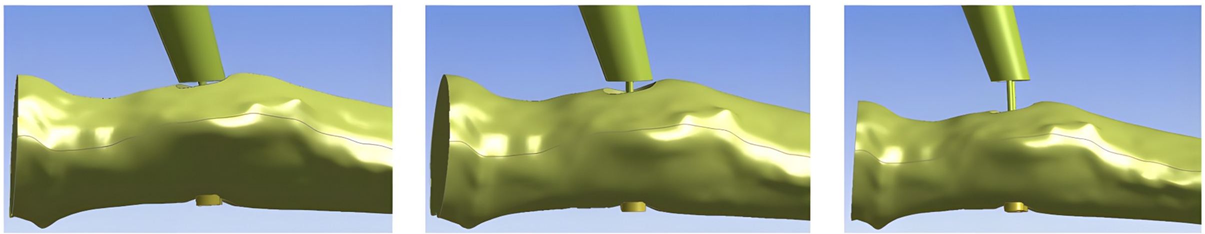

a) b) c)

Fig. 5 Cortical button model for suture fixation. Ellipsoidal titanium button (length 10 mm, width 2.6 mm, thickness 1.5 mm) with two holes (diameter 1.5 mm each) for suture passage, positioned on the posterior radial surface.



Fig. 6 Schematic of model loading. Resultant tensile force applied as uniformly distributed pressure of 500 N vertically upward to the superior tendon boundary, simulating physiological loading from biceps muscle contraction at 90° elbow flexion.

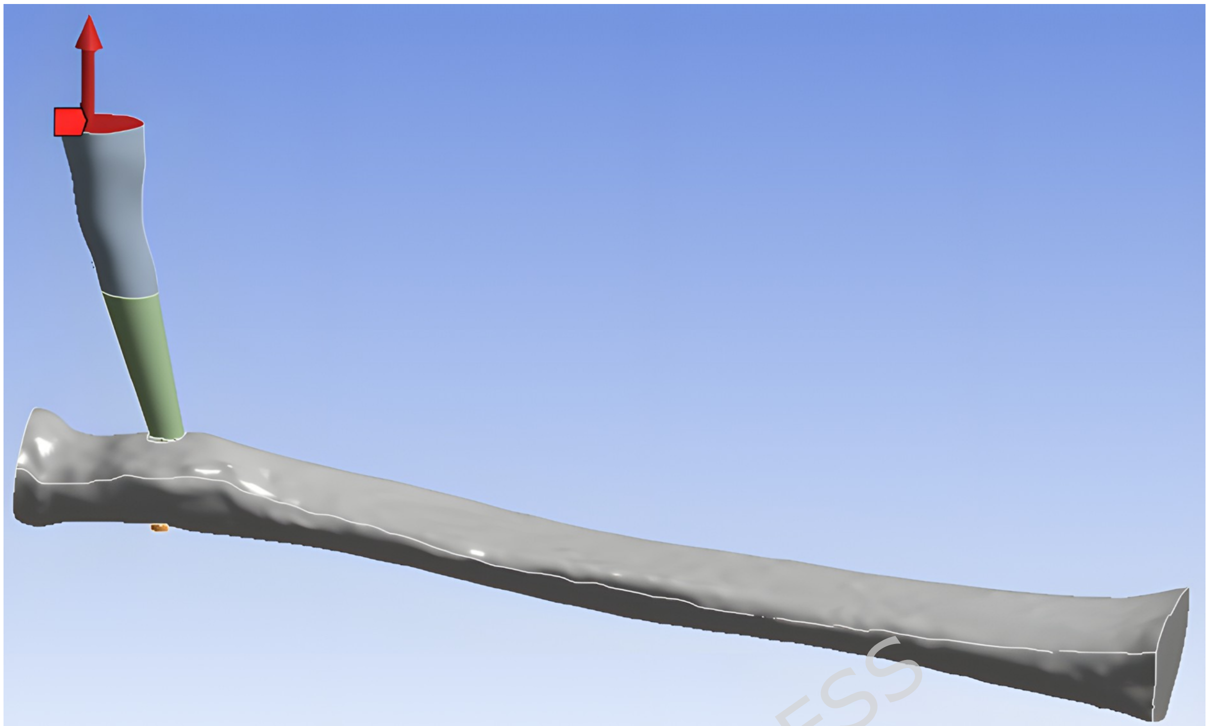

Fig. 7 Coordinate system used in the computational models. XYZ system with X and Y axes in the horizontal plane and Z axis directed vertically from inferior to superior, perpendicular to the XOY plane.



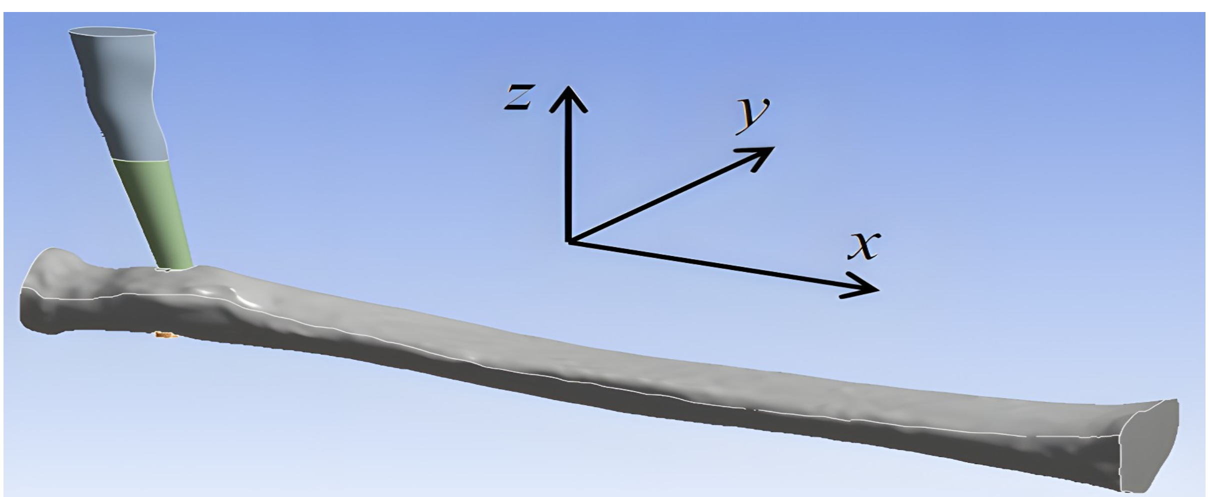

Fig. 8 Finite element mesh of the models. Tetrahedral mesh with maximum element size of 1 mm applied to all components (radius, tendon, fixation system, and button).

Fig. 9 Normal stress (σ_z) distribution patterns.

(a) Fixation system model showing maximum stresses in the suture material portion.

(b) Tendon model with more uniform stress distribution and minor concentration zones in the inferior portion.

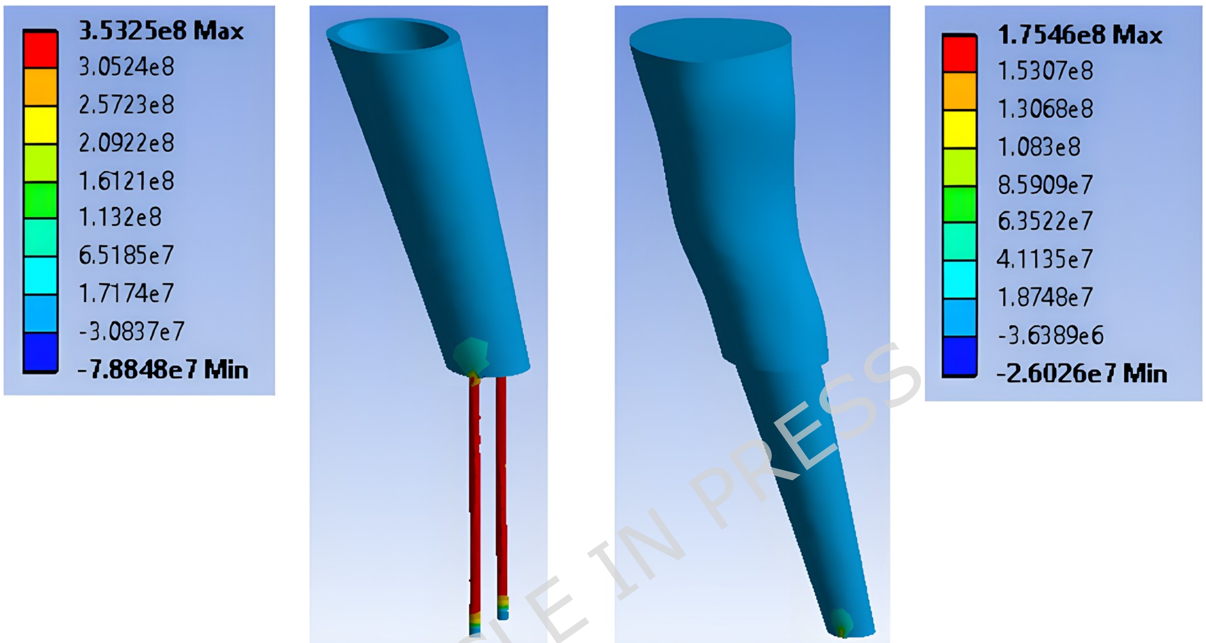


a) b)

Fig. 10 Relative longitudinal strain (ε_z) distribution patterns.

(a) Fixation system model with highest strains in the sutures, decreasing proximally in the whipping section. (b) Tendon model with maximum strains in the distal portion, decreasing proximally.

Fig. 11 Displacement distribution patterns under 500 N load.

(a) Fixation system model showing primary deformation in the suture portion and near-rigid body displacement in the whipping section. (b) Tendon model behaving predominantly as a rigid body with displacements resulting mainly from suture elongation.